Title

A new crystal form of human acetylcholinesterase for exploratory room-temperature crystallography studies

Authors

Gerlits, Oksana
Ho, Kwok-Yiu
Cheng, Xiaolin
et al.

Publication Date

2019-08-01

DOI

10.1016/j.cbi.2019.06.011

Peer reviewed

HHS Public Access

Author manuscript

Chem Biol Interact. Author manuscript; available in PMC 2020 August 25.

Published in final edited form as:

Chem Biol Interact. 2019 August 25; 309: 108698. doi:10.1016/j.cbi.2019.06.011.

A new crystal form of human acetylcholinesterase for exploratory room-temperature crystallography studies

Oksana Gerlits[a], **Kwok-Yiu Ho**[b], **Xiaolin Cheng**[c], **Donald Blumenthal**[d], **Palmer Taylor**[b], **Andrey Kovalevsky**[e], **Zoran Radić**[b,*]

[a]Bredesen Center, University of Tennessee, Knoxville, TN, 37996, USA

[b]Skaggs School of Pharmacy and Pharmaceutical Sciences, University of California San Diego, La Jolla, CA, 92093-0650, USA

[c]Division of Medicinal Chemistry & Pharmacognosy, College of Pharmacy, The Ohio State University, Columbus, OH, 43210, USA

[d]Department of Pharmacology and Toxicology, University of Utah, Salt Lake City, UT, 84112, USA

[e]Neutron Scattering Division, Oak Ridge National Laboratory, Oak Ridge, TN, 37831, USA

Abstract

Structure-guided design of novel pharmacologically active molecules relies at least in part on functionally relevant accuracy of macromolecular structures for template based drug design. Currently, about 95% of all macromolecular X-ray structures available in the PDB (Protein Data Bank) were obtained from diffraction experiments at low, cryogenic temperatures. However, it is known that functionally relevant conformations of both macromolecules and pharmacological ligands can differ at higher, physiological temperatures. We describe in this article development and properties of new human acetylcholinesterase (AChE) crystals of space group $P3_1$ and a new unit cell, amenable for room-temperature X-ray diffraction studies. We co-crystallized hAChE in $P3_1$ unit cell with the reversible inhibitor 9-aminoacridine that binds at the base of the active center gorge in addition to inhibitors that span the full length of the gorge, donepezil (Aricept, E2020) and AChE specific inhibitor BW284c51. Their new low temperature $P3_1$ space group structures appear similar to those previously obtained in the different $P3_121$ unit cell. Successful solution of the new room temperature 3.2 Å resolution structure of BW284c51*hAChE complex from large $P3_1$ crystals enables us to proceed with studying room temperature structures of lower affinity complexes, such as oxime reactivators bound to hAChE, where temperature-related conformational diversity could be expected in both oxime and hAChE, which could lead to better informed structure-based design under conditions approaching physiological temperature.

*Corresponding author. zradic@ucsd.edu (Z. Radić).

Declaration of interests

The authors declare that they have no known competing financial interests or personal relationships that could have appeared to influence the work reported in this paper.

Transparency document

Transparency document related to this article can be found online at https://doi.Org/10.1016/j.cbi.2019.06.011

Keywords

Human acetylcholinesterase; Room-temperature X-ray structure; Structure-based drug design; Donepezil; 9-Aminoacridine; BW284c51

1. Introduction

Structural investigations of acetylcholinesterase (AChE; EC 3.1.1.7) catalytic subunit flourished after its amino acid sequence was deduced from cDNA cloning [1], beginning with the X-ray structure determination of electric ray AChE (*Torpedo californica*, TcAChE) [2] in 1991. In the following decades more than two hundred AChE structures have been deposited into the Protein Data Bank (PDB). The first solved TcAChE structure represented a breakthrough in understanding the basis of the enzyme's highly evolved catalytic mechanism and provided a 3D template for design of therapeutically important inhibitors, such as donepezil (Aricept, E2020) [3], for partial symptomatic treatment of Alzheimer's disease. This structure also informed the design of oxime antidotes for reactivation of AChE covalently inhibited by organophosphate pesticides and chemical warfare agents. Nearly 95% of all PDB X-ray depositions (~152,500 as of June 2019), including practically all AChE structures, have been obtained from the diffraction experiments run at cryogenic temperatures, 210 °C below human body temperature. Among the AChE structures, less than 20% are structures of therapeutically appropriate, human AChE (hAChE) target.

The benefits of cryogenic X-ray data collection arise from reduced radiation damage of crystal allowing for high dataset completeness, improved resolution of the diffraction image and good accuracy of resulting atomic coordinates. Our goal is to explore the feasibility of hAChE structural analysis under conditions closer to physiological conditions (37 °C or 310 K) and to use room temperature X-ray data collection (at 22 °C or 295 K), instead of cryogenic temperatures (−173 °C or 100 K). While potentially sacrificing higher resolutions typically obtained at cryogenic temperature our hope is to gain better insight of a range of physiologically more relevant protein conformations indicative of structural flexibility, while also avoiding protein crystal flash freezing and use of cryoprotectants which are known to harm X-ray diffraction quality and interfere with small molecule ligand binding [4]. One way of counteracting crystal damage associated with X-ray exposure at room temperature is to perform diffraction using large, high-quality crystals capable of producing complete diffraction datasets before the radiation causes substantial degradation. Using a hAChE construct lacking one of the protein's three glycosylation sites, we have been able to grow larger than usual crystals of human AChE in the $P3_1$ space group. These larger crystals are able to better withstand radiation damage at room temperature and allow for the collection of reasonably complete datasets with acceptable resolution of the final X-ray structure. Unlike previously characterized hAChE crystals (most belonging to $P3_121$ space group and a few to H32, P6, $P6_1$ or $P2_1$ space groups) the unit cell dimensions of the $P3_1$ hAChE crystals appear similar ($a = b \cong c$). These crystals can grow ~250 times larger than the previously reported crystals and diffract well at room temperature. In the asymmetric subunit of the $P3_1$ form two kinds of hAChE homodimers are observed: the commonly found four-helix bundle (4HB) dimer and a “face-to-face” (FF) dimer. Due to the absence of one of the three hAChE

glycosylation sites, the two monomers can establish a dimerization interface close to the opening of the hAChE active center gorge in the FF dimer. This dimer formation does not interfere with ligand access to the active center gorge, thus allowing entrance of small molecules during soaking experiments. We present here the structures of hAChE in space group $P3_1$ at room temperature in complex with the specific reversible AChE inhibitor BW284c51, and at low temperature in complexes with the drug donepezil (Aricept, E2020), with BW284c51 and with 9-aminoacridine, a congener of the drug tacrine (Cognex). Comparison of these structures with published structures reveals nearly identical positions of those ligands in the active center gorges of TcAChE and in different crystal forms of hAChE, thus confirming that the $P3_1$ hAChE form represents a valid structural template for low temperature studies, and can serve to explore X-ray analysis of hAChE structure under conditions approaching physiological temperature.

2. Materials and methods

Protein expression and purification.

Human AChE was expressed in monomeric form truncated at C-terminal amino acid 547 and with a FLAG tag placed at the N-terminal end [5]. Stably transfected $Gnt1^-$ HEK293 mammalian cell culture deficient in complex N-glycans was used for expression. Cells were grown at 37 °C and 10% CO_2 in Dulbecco's modified Eagle's medium, containing 10% fetal bovine serum. The enzyme was purified on an anti-FLAG affinity chromatography column (Sigma-Aldrich) using proteolytic elution by specific Recombinant HRV 3C protease (Sinobiological.com) at the engineered Prescission protease recognition site. Profinity IMAC Resin (Bio Rad) was used to remove the HRV 3C protease. The N-terminal sequence of the purified, eluted hAChE was G-P-L-**E-G-R-**. The amino acid sequence of the mature hAChE protein starts at **E-G-R-** and ends at the truncated C-terminus [5] with the sequence -S-A-T-D-T-L-D^{547}.

Crystallization.

Ligands, donepezil, 9-aminoacridine and BW284c51 were obtained from Sigma-Aldrich and 30–60 mM stock solutions were prepared in DMSO. In preparation for co-crystallization, samples of hAChE were dialyzed in 10 mM NaCl, 10 mM HEPES, pH 7, and concentrated to 6–10 mg/mL. About 1 h prior to crystallization, the solution of hAChE was combined with stock solutions of ligands in a molar ratio of 1:5 or 1:10 to obtain binary complexes. Co-crystals were grown by vapor diffusion at 10 °C in sitting drop microbridges or 9-well glass plates (Hampton Research, Aliso Viejo, CA). Well solutions containing 10 mM sodium citrate, 100 mM HEPES, pH 7.5, 7–12% PEG6000 were used in crystallization experiments with donepezil and BW284c51 and 200 mM potassium nitrate, 100 mM HEPES pH 7.5, 9% PEG 3350 were used to produce crystals with 9-aminoacridine. Crystals typically appeared within 2-4 weeks (~0.1-0.2 mm in the longest dimension) and over 2-4 months, depending on the ligand, slowly grew to full size (> 1 mm). Largest crystals were observed in drops that contained 1-3 crystals.

X-ray data collection.

X-ray crystallographic data were collected at room temperature (~22 °C; RT) and from frozen crystals at 100 K. Prior to data collection at 100 K crystals were subjected to two very brief consecutive soaks in the cryoprotectant solutions, first in 12% glycerol followed by 25% glycerol, and then flash cooled by plunging into liquid nitrogen. For the RT data collection, crystals were mounted on Litholoops (Molecular Dimensions, Maumee, OH) directly from the crystallization or soaking drops and kept hydrated using the MiTeGen (Ithaca, NY) room temperature setup. Diffraction data were collected on the ID19 (100 K) and BM19 (293 K) beamlines at SBC-CAT using Pilatus3 X 6 M (ID19) and MAR CCD 165 mm (BM19) detectors at the Advanced Photon Source (APS). X-ray diffraction data were integrated and scaled using the HKL3000 software suite [6]. The structures were solved by molecular replacement using the CCP4 suite [7]. The structure of the apo-hAChE (PDB ID 4EY4) [8] was used as a starting model with all waters and the *N*-linked glycosylated saccharides removed. Refinement was performed using the *phenix.refine* program in the *PHENIX* [9] suite and the resulting structure analyzed with *molprobity* [10]. The structures were built and manipulated with the program *Coot* [11]. Figures were generated using *Coot, Biovia Discovery Visualizer* (Dassault Systems) and *PyMol* molecular graphics software (Schrödlnger LLC). A summary of the crystallographic data and refinements is given in Table 1. Crystallographic data have been deposited to PDB under codes 6O4W (donepezil*hAChE), 6O4X (9-aminoacridine*hAChE), 6O50 (LT: BW284c51*hAChE) and 6O52 (RT: BW284c51c*hAChE).

3. Results and discussion

3.1. New crystal form of hAChE

Human AChE truncated at the amino acid residue 547 was expressed in a HEK-293 cell line as a monomeric form [5] and is devoid of the N-linked oligosaccharide chain at position 350. While none of the three glycosylation sites (265, 350 and 464) appeared clear enough in the electron density maps to be unequivocally modelled, the absence of an expected oligosaccharide at 350 was obvious from both complete absence of electron density and as inferred from the immediate proximity of the neighboring chain of the homodimer which would be incompatible with oligosaccharide at Asn350 (Fig. 1).

Glycosylation of Asn350 is clearly visible in published hAChE structures that crystallize in a $P3_121$ space group, for example in 4EY7 (Fig. 1) [8]. Our construct thus forms two distinct dimers in the crystal, one stabilized by the C terminal 4HB dimer interaction and the other one by “face-to-face” interaction of the two subunits near Asn350 in the general vicinity of the two active center gorge openings. Areas and solvation energies of dimer interfaces calculated by the PISA server [12,13] show clear dominance of 4HB dimer interactions, but also significant contribution of the face-to-face interface in the $P3_1$ dimer (Table 2).

It is interesting that in the $P3_1$ packing the energetically most stabilizing 4HB dimer interactions (red helices in Fig. 2) are distributed both horizontally and vertically in a 3D network unlike that seen in $P3_121$ packing where only 2D, horizontal layers of hydrophobic “sticky” interactions are formed.

As a result of this homodimer packing, our $P3_1$ crystals are more compact with unit cell dimensions a = 125.18 Å, b = 125.18 Å, c = 130.28 Å, in contrast to hAChE 4EY7 $P3_121$ crystals which have more elongated needle-like appearance (a = 105.15 Å, b = 105.15 Å, c = 322.98 Å) [8]. The influence of glycosylation on crystal packing is further seen in the complex of donepezil with fish TcAChE (PDB code 1EVE) where a different distribution of four glycosylation sites prevents formation of FF dimers, while 4HB dimer interaction remains (Table 2). Instead of FF dimers, a new, less stabilizing face-to-back (FB) dimer is formed (Fig. 1; Table 2) resulting in the 3D distribution of most hydrophobic "sticky" interactions (Fig. 2), but a less compact crystal (a = 111.93 Å, b = 111.93 Å, c = 136.90 Å) [3], The compact $P3_1$ hAChE packing is amenable to forming large, more than 1 mm long stick-like crystals (Image 1) with good quality X-ray diffraction properties critical for data collection under conditions of high radiation damage in a room temperature X-ray diffraction experiment.

3.2. Low temperature complexes of $P3_1$ hAChE with reversible ligands

All three reversible ligands, donepezil (E2020), BW28451c (BW) and 9-aminoacridine (9AA) classify as low nanomolar AChE inhibitors (Table 3) and co-crystalize with hAChE in the same $P3_1$ space group with a nearly identical relative orientation of monomers in a 4HB dimer (Fig. 3). A barely distinguishable monomer tilt observed in 9AA and BW complexes compared to E2020 complex (Fig. 3A) seems to indicate only slightly more compact dimers for the donepezil*hAChE complex (black and blue graphs, Fig. 3B) as indicated by differential distance analysis between corresponding amino acid Cα atoms of individual homodimers [18]. This is also reflected in the Cα-based rigid body dimer overlay (Table 4).

Donepezil*hAChE low temperature complex.—The positioning of the *S* enantiomer of donepezil in our co-crystals is identical to the one found in hAChE co-crystals in 4EY7 [8] (RMSD = 0.3 Å for heavy atoms of the donepezil molecules), based on Cα atom overlays of four hAChE monomers (two monomer chains from each structure) (Fig. 4). Bound donepezil, fully resolved by electron density maps is stabilized in the $P3_1$ hAChE (6O4W) active center gorge by precisely the same interactions (Fig. 4) as observed in 4EY7 [8]. This is despite noticeable monomer tilt in the 4EY7 dimers compared to our structure (revealed by mismatch in yellow and teal colored dimer ribbons and associated green graph of the differential distance analysis in Fig. 3) and the presence of the FF dimers in the $P3_1$ structure in the general vicinity of the bound donepezil. The observed quaternary structure differences, thus, did not influence binding of the slender donepezil molecule which spans the base and the opening of the hAChE active center gorge in precisely the same manner in all structures. Donepezil is stabilized (Fig. 4) by stacking interactions with aromatic rings of Trp 86, Trp 286, Tyr337 and Phe338, hydrophobic interactions with Tyr341, and hydrogen bonds with backbone carbonyls of Ser293 and Phe295, and hydroxyl of Tyr72. It also hydrogen bonds to five water molecules in the immediate vicinity, H_2O water molecules 34, 88, 155, 157 and 260. Consistent with previous observations [8] the binding is somewhat different in the donepezil*TcAChE complex (1EVE) obtained by soaking, with a slight tilt of the plane of the peripheral 5,6-dimethoxy-2,3dihydroinden-1-one ring and a flip of the central piperidine ring. Neither of the two structures are affected by the observed quaternary

structure level differences (Fig. 1) between the $P3_1$ donepezil*hAChE complex 6O4W and the 4EY7 and 1EVE structures of the same complex.

9-Aminoacridine*hAChE low temperature complex.—This is the first structure of 9AA, a congener of the initial Alzheimer's disease drug tacrine (Cognex) in complex with an AChE. Complexes of tacrine with TcAChE (1ACJ) and human BChE (4BDS) have been previously published [19,20]. The only difference between 9AA and tacrine is that in tacrine one of the benzene rings of 9AA is fully saturated. Their binding affinities for AChE are less than two-fold different (Table 3) [15], as is also the case for BChE [14]. Fully resolved by electron density maps 9AA binds at the base of the hAChE active center gorge establishing close stacking interactions between the tricyclic aromatic ring and Trp86 on one side and with Tyr337 on the other side forming a nearly equidistant π orbital sandwich (Fig. 5). Additional weaker stacking stabilization is provided by the 5.8 Å distant imidazole of the catalytic triad His447. Tacrine is stabilized in TcAChE and human BChE (1ACJ and 4BDS structures) in virtually the same position by stacking interactions with Trp86 but the His447 stacking is missing due to ring saturation in tacrine (Fig. 5). A slight ~0.6 Å shift of 9AA towards Ser203 compared to tacrine is consequently observed (Fig. 5). In all three structures, amino groups of both 9AA and tacrine form hydrogen bonds with two adjacent water molecules.

BW284c51*hAChE low temperature complex.—The AChE-selective inhibitor BW284c51, similarly to donepezil, spans the active center gorge of hAChE between Trp86 at the base and Trp286 at the gorge opening. The two inhibitors are similar in size and have similar inhibition constants in the low nanomolar range, yet they are stabilized differently in the gorge of different AChEs. In the hAChE structure 6O50, BW284c51as a symmetric, charged *bis*-quaternary compound, primarily forms cation-π and π-π interactions between its terminal exocyclic quaternary nitrogens and aromatic rings of Trp86 and Trp286 (Fig. 6), a Coulombic attraction to Glu202, and aromatic hydrophobic π-π stacking of its lower aromatic ring with Tyr337 and upper aromatic ring with Trp286. The terminal alkenes of BW284c51 are additionally stabilized by Tyr337 and Tyr449 at the gorge base and by Leu76 at the gorge opening. In the published complex of BW284c51 with TcAChE (PDB:1E3Q) [21] the lower half of the ligand is nearly identically stabilized at the aromatic gorge base, but the upper benzene ring is drawn by 1–1.5 Å deeper into the gorge to curl (Fig. 6) and establish an additional weak, hydrophobic π-π sandwich between ~5 π distant rings of Trp279 and Tyr334 at the peripheral site (homologous to Trp 286 and Tyr341 in hAChE).

In our BW284c51*hAChE co-crystalized complex the ligand, fully resolved by electron density maps, extended by ~1 Å farther outside of the gorge than in the BW284c51*TcAChE complex obtained by soaking. This is even ~1.7 Å farther out than the extension of donepezil in its hAChE or TcAChE complexes. In TcAChE both BW284c51 and donepezil extend similarly far outside of the TcAChE gorge, both significantly less than BW284c51 in our hAChE complex. This may reflect steric occlusion caused by the symmetry-related TcAChE molecule in the crystal packing, restricting access at the active center gorge opening by the associated FB dimer. Indeed, the closest residue of the symmetry-associated FB monomer to the bound BW284c51 of 1E3Q is His181, only 3.9 Å

away, serving as a steric and possibly also electrostatic obstacle to relaxed ligand binding for the $P3_121$ TcAChE complexes. In our $P3_1$ hAChE complexes with 4HB and FF dimers, we do not observe this kind of limitation imposed by crystal packing. In fact, we note very fast ligand soaking into this $P3_1$ crystal form of hAChE (Gerlits et al., J. Biol. Chem. 2019, *in press*).

3.3. Room temperature structure of the BW284c51*hAChE complex

The unique properties of the novel $P3_1$ crystal packing of hAChE allowed us to grow about $1.5 \times 0.2 \times 0.2$ mm^3 crystals suitable for X-ray data collection at room temperature (Image 1), without the need to use cryoprotectants and flash freezing of crystals both of which can introduce structural artifacts [4]. We were able to collect a sufficiently complete room temperature X-ray diffraction data set and solve an RT structure of the BW284c51*hAChE complex at the 3.2 Å resolution (6O52; Table 1). The resulting electron density of the RT structure looks surprisingly well-defined and similar to the higher resolution 2.4 Å structure of the same complex collected under LT conditions (6O50; Figs. 7 and 8), perhaps due to the high binding affinity of BW284c51, allowing for their comparison. Ligand conformation and position, and hAChE backbone and sidechain conformations, in both LT and RT structures appear nearly identical, particularly within the active center gorge (Fig. 7). The exception is a relatively small local surface loop difference (with up to 2.4 Å deviations for residues 261–265). In the more detailed differential distance analysis using Ser203 as a frame of reference [18] the overall difference in Cα positions between RT and LT structures appeared slightly larger than the difference between the two monomers from homodimers in the same LT structure (red vs grey traces, Fig. 7C). In fact, the difference between the two LT structures, the one of 9AA*hAChE (6O4X) compared to the BW284c51*hAChE (6O50) complex (black vs grey traces in Fig. 7 graph), appears slightly larger. This may not be surprising for a tight binding of a low nM inhibitor such as BW284c51, which fills the hAChE active center gorge fully, thus stabilizing both ligand and protein conformations, at both LT and RT. The two largest peaks of difference between 9AA and BW284c51 LT complexes correspond to the Ω loop (residues 69–96) and α-helical residue stretch between 337 and 350 (Fig. 7C) that structurally represent the active center gorge lid and the upper gorge “floor”. Both of these structural elements participate in stabilization of bound BW284c51 (Fig. 6), but not of the much smaller 9AA that occupies only the base of the gorge (Fig. 5). Hence, the upper part of the gorge opens up slightly even at LT in the 9AA complex, when compared to the BW284c51 LT complex.

3.4. Comparison of structures at the tertiary and quaternary levels

Using protein backbone α-carbon-based overlays and resulting RMSD values as criteria, we compared effects of data collection temperature and unit cell symmetry for hAChEs as well as primary sequence differences between hAChE and TcAChE, on the similarity of their monomeric tertiary structure folds and similarity in organization of monomers into 4HB dimeric quaternary structure (Tables 4 and 5). Total of nine structures were included in the comparison. Four of them were $P3_1$ hAChEs from this study and four were previously published $P3_121$ complexes of donepezil, tacrine and BW284c51 with TcAChE and hAChE. The human BChE*tacrine complex was also included in the comparison because of the similarity in the BChE backbone fold with AChEs and because of the similar, yet distinct

4HB quaternary organization in the two enzymes. While the resolution of the structures may not allow for a detailed statistical analysis, several obvious “out of range” value comparisons are readily noticeable.

The effect of diffraction data collection temperature seemed slightly larger on the hAChE tertiary structure than on the quaternary organization of its 4HB homodimer. The 4HB dimer of the BW284c51 RT complex (6O52) overlaid with the LT complex (6O50) had a relatively small RMSD of 0.38 Å (Table 4). When compared to other $P3_1$ hAChE LT complexes from Table 4 (numbers in the yellow box), the RMSD ranged from 0.38 Å to 0.63 Å. This was only slightly more than the 0.37 Å to 0.49 Å RMSD range determined for comparison of the same structures with the 4HB dimer of the BW284c51 LT complex. When quaternary comparison was extended to the $P3_121$ dimer of the 4EY7 hAChE and $P3_121$ TcAChE dimers, no difference can be observed between LT and RT complexes (magenta box in Table 4). Temperature-dependent tertiary structural differences revealed from comparison of monomers were, however, larger (Table 5). The comparison of BW $P3_1$ hAChE monomers to all other $P3_1$ monomers (within the yellow box in Table 5) shows a RMSD range of 0.34 Å to 0.42 Å for the RT complex but a noticeably smaller 0.24 Å - 0.30 Å range for the LT complex. An extension of the tertiary structural comparison to $P3_121$ monomers of the 4EY7 hAChE and $P3_121$ TcAChE monomers, revealed no difference between LT and RT complexes (magenta box in Table 5). Effectively, while RMSD numbers in the two rows in Table 5 corresponding to RT structures were noticeably larger than other numbers within the yellow box of Table 5 (0.34 Å - 0.43 Å vs. 0.26 Å - 0.31 Å; excluding a to b chain comparisons of the same structure), the same did not hold for RMSD values within the magenta box of Table 4 (0.48 Å – 0.92 Å vs. 0.46 Å - 0.94 Å). In conclusion, the effect of temperature was observed only for small RMSD values (≤ 3 Å) when comparing monomer folds within the same $P3_1$ space group, but the quaternary structures were not noticeably affected by temperature.

The effect of unit cell symmetry change from $P3_1$ to $P3_121$ for hAChE is emphasized at the quaternary level where 4EY7 hAChE dimers differ from 4HB dimers of $P3_1$ hAChE structures by 1.45–1.52 Å RMSD whereas comparison of monomers yields only 0.46–0.53 Å RMSD. It is interesting that the $P3_121$ dimers of the tacrine*TcAChE complex (1ACJ) show noticeably greater similarity with $P3_1$ dimers (0.90–1.06 Å RMSD) than the other two $P3_121$ TcAChE complexes containing much longer ligands, donepezil (1EVE, 1.48–1.56 Å RMSD) and BW284c51 (1E3Q, 1.46–1.62 Å RMSD). In addition to binding in the active center gorge these longer ligands also occupy peripheral site at the mouth of the TcAChE gorge. Thus the greater effect of unit cell symmetry might be a consequence of the pressure of peripherally bound ligands on tight packing of FB TcAChE dimers (Table 2; Fig. 1) that also had an effect on the more “curled” conformation of BW284c51 in the $P3_121$ TcAChE complex (1E3Q) compared to its $P3_1$ hAChE complex (6O50) shown in Fig. 6C.

The effect of primary sequence differences on quaternary and tertiary AChE structure is illustrated by cross-species comparisons between hAChE and TcAChE within the same $P3_121$ space group (teal boxes in Tables 4 and 5). A larger magnitude RMSD difference is observed in quaternary structure comparisons between species relative to those within species (0.96–1.45 Å between hAChE and TcAChE dimers vs. 0.32–0.59 Å within TcAChE

dimers). The difference was also significant for the tertiary structure comparisons (0.93–0.97 Å between hAChE and TcAChE dimers vs. 0.32–0.39 Å within TcAChE dimers). Thus, both monomers and dimers are different between AChEs from different species although they crystalize in the same space group.

Comparisons of AChEs with the human BChE*tacrine complex (4BDS) reveal two interesting points. The BChE tertiary backbone structure was similarly distinct to that of both TcAChE and hAChE structures with ~1.1 Å RMSDs (Table 5) which is relatively close to comparisons of TcAChE vs. hAChE (~0.9 Å RMSDs). The BChE quaternary structure was, however, clearly distinct from those observed in AChEs (~3 Å RMSDs; Table 4). Still, it appears that 4HB dimers of BChE were more similar to 4HB dimers of $P3_1$ hAChE (~2.7 Å RMSD) than to P3121 4HB dimers (3.23 Å – 3.57 Å RMSD). The exception is the $P3_121$ TcAChE*tacrine dimer (1ACJ) which had a 2.75 Å RMSD (Table 4). It seems that the size of a ligand (small tacrine or 9-aminoacridine vs. large donepezil (E2020) or BW284c51) and its binding site within the active center gorge of either AChE or BChE could influence, at least modestly, the quaternary structures of these enzymes.

4. Conclusions

Crystallogenesis from a glycosylation-deficient form of hAChE yields relatively large (1.5 mm × 0.2 mm × 0.2 mm) crystals of space group $P3_1$ and a new unit cell, not previously obtained for AChE from any species. Specific arrangement of monomers in the $P3_1$ hAChE crystals simultaneously includes two kinds of homodimers, the previously observed 4HB dimer and a novel FF dimer, thus creating a compact 3D packing amenable to formation of large, well-diffracting crystals suitable for RT X-ray crystallography.

Co-crystallization of hAChE-ligand complexes in the $P3_1$ unit cell with ligands binding to either the base of the active center gorge or with those spanning its full length were not affected by FF dimer formation and revealed LT X-ray structures nearly identical to those obtained in previous LT X-ray structures. The $P3_1$ hAChE crystals are readily amenable to soaking by ligands of the shape and size used in this study.

Successful determination of a RT hAChE structure at 3.2 Å from large $P3_1$ crystals of BW284c51*hAChE complex lays the groundwork for future comprehensive studies of RT structures of lower affinity complexes, such as oxime reactivators associated with hAChE, where more temperature-related diversity could be expected in both oxime and hAChE conformations (Gerlits et al., J. Biol. Chem. 2019, *in press*) to better inform structure-based design of novel reactivators of hAChE under conditions approaching physiological temperature.

Supplementary Material

Refer to Web version on PubMed Central for supplementary material.

Acknowledgments

X-ray crystallographic data presented in this report are derived from work performed at Argonne National Laboratory, Structural Biology Center (SBC) at the Advanced Photon Source. Use of the Advanced Photon Source,

an Office of Science User Facility operated for the U.S. Department of Energy (DOE) Office of Science by Argonne National Laboratory, was supported by the USDOE under Contract No. DE-AC02-06CH11357. The Office of Biological and Environmental Research supported research at the Center for Structural Molecular Biology (CSMB) at ORNL using facilities supported by the Scientific User Facilities Division, Office of Basic Energy Sciences, U.S. Department of Energy.

Funding

This research was supported by the CounterACT Program, National Institutes of Health Office of the Director (NIH OD), and the National Institute of Neurological Disorders and Stroke, [Grant Numbers U01 NS083451 and R21 NS098998].

References

[1]. Schumacher M, Camp S, Maulet Y, Newton M, MacPhee-Quigley K, Taylor SS, Friedmann T, Taylor P, Primary structure of *Torpedo californica* acetylcholinesterase deduced from its cDNA sequence, Nature 319 (1986) 407–409. [PubMed: 3753747]

[2]. Sussman JL, Harel M, Frolow F, Oefner C, Goldman A, Toker L, Silman I, Atomic structure of acetylcholinesterase from *Torpedo californica*: a prototypic acetylcholine-binding protein, Science 253 (1991) 872–879. [PubMed: 1678899]

[3]. Kryger G1, Silman I, Sussman JL, Structure of acetylcholinesterase complexed with E2020 (Aricept): implications for the design of new anti-Alzheimer drugs, Structure 7 (1999) 297–307. [PubMed: 10368299]

[4]. Dym O, Song W, Felder C, Roth E, Shnyrov V, Ashani Y, Xu Y, Joosten RP, Weiner L, Sussman JL, Silman I, The impact of crystallization conditions on structure-based drug design: a case study on the methylene blue/acetylcholinesterase complex, Protein Sci. 25 (2016) 1096–1114. [PubMed: 26990888]

[5]. Cochran R, Kalisiak J, Küçükkilinç T, Radic Z, Garcia E, Zhang L, Ho KY, Amitai G, Kovarik Z, Fokin VV, Sharpless KB, Taylor P, Oxime-assisted acetylcholinesterase catalytic scavengers of organophosphates that resist aging, J. Biol. Chem 286 (2011) 29718–29724. [PubMed: 21730071]

[6]. Minor W, Cymborowski M, Otwinowski Z, Chruszcz M, HKL-3000: the integration of data reduction and structure solution–from diffraction images to an initial model in minutes, Acta Crystallogr. D 62 (2006) 859–866. [PubMed: 16855301]

[7]. C.P. Collaborative, The CCP4 suite: programs for protein crystallography, Acta Crystallogr. D 50 (1994) 760–763. [PubMed: 15299374]

[8]. Cheung J, Rudolph MJ, Burshteyn F, Cassidy MS, Gary EN, Love J, Franklin MC, Height JJ, Structures of human acetylcholinesterase in complex with pharmacologically important ligands, J. Med. Chem 55 (2012) 10282–10286. [PubMed: 23035744]

[9]. Adams PD, Afonine PV, Bunkóczi G, Chen VB, Davis IW, Echols N, Headd JJ, Hung L-W, Kapral GJ, Grosse-Kunstleve RW, PHENIX: a comprehensive Python-based system for macromolecular structure solution, Acta Crystallogr. D 66 (2010) 213–221. [PubMed: 20124702]

[10]. Davis IW, Leaver-Fay A, Chen VB, Block JN, Kapral GJ, Wang X, Murray LW, Arendall WB, Snoeyink J, Richardson JS, MolProbity: all-atom contacts and structure validation for proteins and nucleic acids, Nucleic Acids Res. 35 (2007) W375–W383. [PubMed: 17452350]

[11]. Emsley P, Lohkamp B, Scott WG, Cowtan K, Features and development of Coot, Acta Crystallogr. D 66 (2010) 486–501. [PubMed: 20383002]

[12]. "Protein interfaces, surfaces and assemblies" service PISA at the European Bioinformatics Institute, (http://www.ebi.ac.uk/pdbe/prot_int/pistart.html).

[13]. Krissinel E, Henrick K, Inference of macromolecular assemblies from crystalline state, J. Mol. Biol 372 (2007) 774–797. [PubMed: 17681537]

[14]. Radić Z, Pickering NA, Vellom DC, Camp S, Taylor P, Three distinct domains in the cholinesterase molecule confer selectivity for acetyl- and butyrylcholinesterase inhibitors, Biochemistry 32 (1993) 12074–12084. [PubMed: 8218285]

[15]. Radić Z, Taylor P, Interaction kinetics of reversible inhibitors and substrates with acetylcholinesterase and its fasciculin 2 complex, J. Biol. Chem 276 (2001) 4622–4633. [PubMed: 11036076]

[16]. Rodrigues Simões MC, Dias Viegas FP, Moreira MS, de Freitas Silva M, Riquiel MM, da Rosa PM, Castelli MR, dos Santos MH, Soares MG, Viegas C Jr., Donepezil: an important prototype to the design of new drug candidates for Alzheimer's disease, Mini Rev. Med. Chem 14 (2014) 2–19. [PubMed: 24251806]

[17]. Darvesh S, Reid GA, Martin E, Biochemical and histochemical comparison of cholinesterases in normal and Alzheimer Brain Tissues, Curr. Alzheimer Res 7 (2010) 386–400. [PubMed: 19939227]

[18]. Rohrer J, Sidhom M, Han J, Radić Z, Overlay-independent comparisons of X-ray structures reveal small, systematic conformational changes in liganded acetylcholinesterase, Period. Biol 118 (2016) 5–14.

[19]. Harel M, Schalk I, Ehret-Sabatier L, Bouet F, Goeldner M, Hirth C, Axelsen PH, Silman I, Sussman JL, Quaternary ligand binding to aromatic residues in the active-site gorge of acetylcholinesterase, Proc. Natl. Acad. Sci. U. S. A 90 (1993) 9031–9035. [PubMed: 8415649]

[20]. Nachon F1, Carletti E, Ronco C, Trovaslet M, Nicolet Y, Jean L, Renard PY, Crystal structures of human cholinesterases in complex with huprine W and tacrine: elements of specificity for anti-Alzheimer's drugs targeting acetyl- and butyrylcholinesterase, Biochem. J 453 (2013) 393–399. [PubMed: 23679855]

[21]. Felder CE, Harel M, Silman I, Sussman JL, Structure of a complex of the potent and specific inhibitor BW284C51 with Torpedo californica acetylcholinesterase, Acta Crystallogr. Sect. D Biol. Crystallogr 58 (2002) 1765–1771. [PubMed: 12351819]

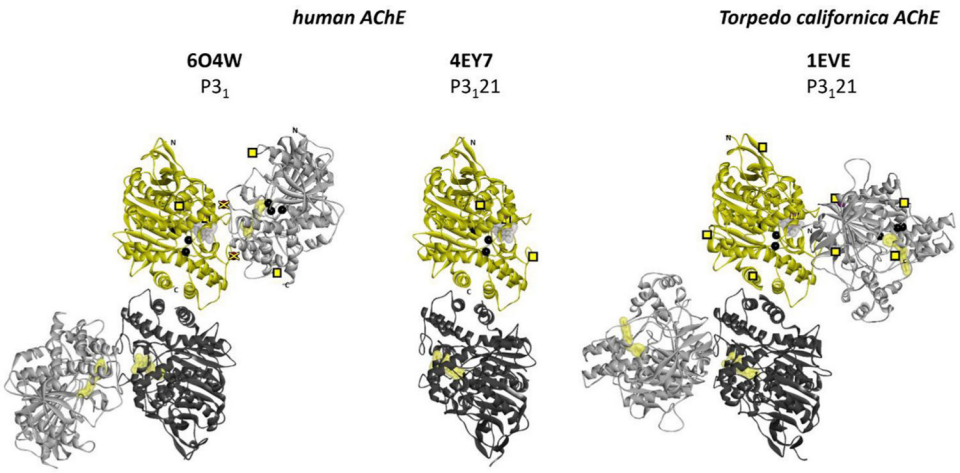

Fig. 1.

Homodimers of the donepezil*hAChE complex found in the P3$_1$ space group structure compared to published P3$_1$21 space group complexes of human (4EY7) and *Torpedo californica* AChE (1EVE). The physiological four-helix bundle (4HB) dimer is found in all three structures. The additional face-to-face dimer is found in the P3$_1$ hAChE complex and is differently oriented in the face-to-back dimer in the TcAChE 1EVE complex. Black spheres indicate the positions of the Ser-His-Glu catalytic triad, yellow squares represent observed glycosylation sites, and yellow crosses mark glycosylation sites absent in the P3$_1$ hAChE complex. Bound donepezil is rendered with a grey or yellow semitransparent Connolly surface to illustrate the active center gorge location. (For interpretation of the references to color in this figure legend, the reader is referred to the Web version of this article.)

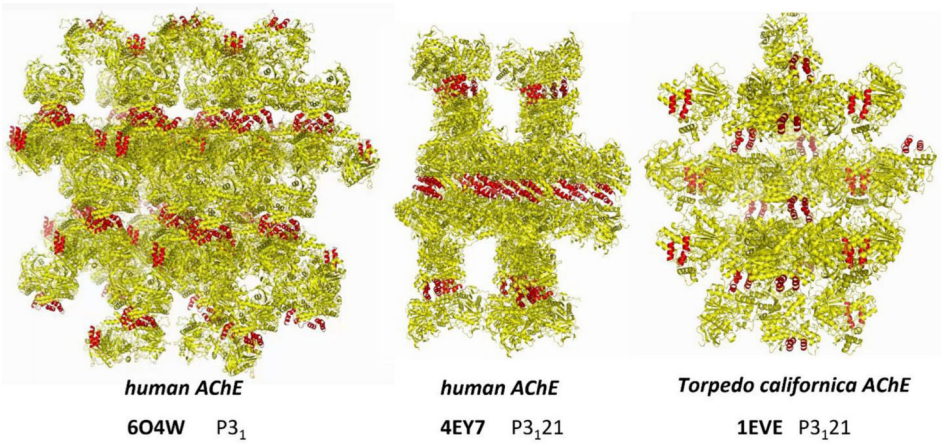

Fig. 2.

Homodimer packing in crystals of three donepezil*AChE complexes from Fig. 1. The 4HB dimerization α-helices are colored red. Symmetry-related AChE subunits were generated from the hAChE 6O4W, hAChE 4EY7 and TcAChE 1EVE structures using PyMOL. (For interpretation of the references to color in this figure legend, the reader is referred to the Web version of this article.)

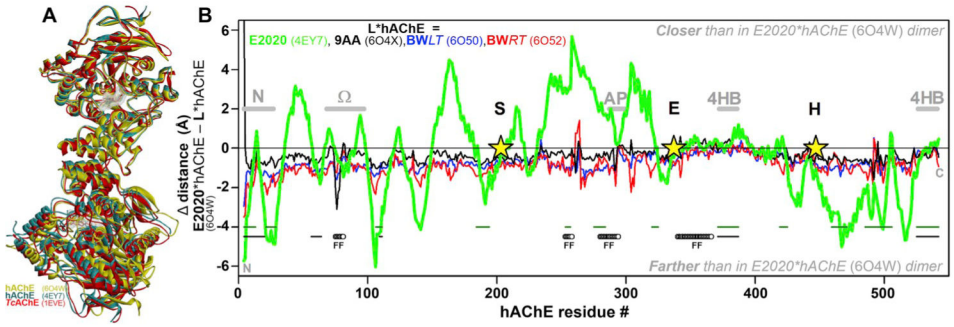

Fig. 3.

A) Overlay of 4HB dimers from three donepezil*AChE complexes from Fig. 1. Dimers are rendered as yellow ribbon ($P3_1$ hAChE complex 6O4W), teal ribbon ($P3_121$ hAChE complex 4EY7) and red ribbon ($P3_121$ TcAChE complex 1EVE). Ribbons of $P3_1$ hAChE LT complexes with 9AA and BW284c51 and RT hAChE complex with BW284c51 are hidden underneath the yellow ribbon. **B)** For **hAChE** dimers the graph indicates change in relative position of monomers in each 4HBD based on differences in distances between corresponding residues in dimer compared to distances in $P3_1$ donepezil*hAChE (6O4W) 4HBD. Catalytic triad residues are indicated by stars and positions of the Ω loop, acyl pocket loop (AP) and 4HB α-helices (4HB) by horizontal grey bars. Contact residues in crystal packing are indicated by green ($P3_121$) and black ($P3_1$) horizontal lines where residues contributing to the FF interface are separately indicated. (For interpretation of the references to color in this figure legend, the reader is referred to the Web version of this article.)

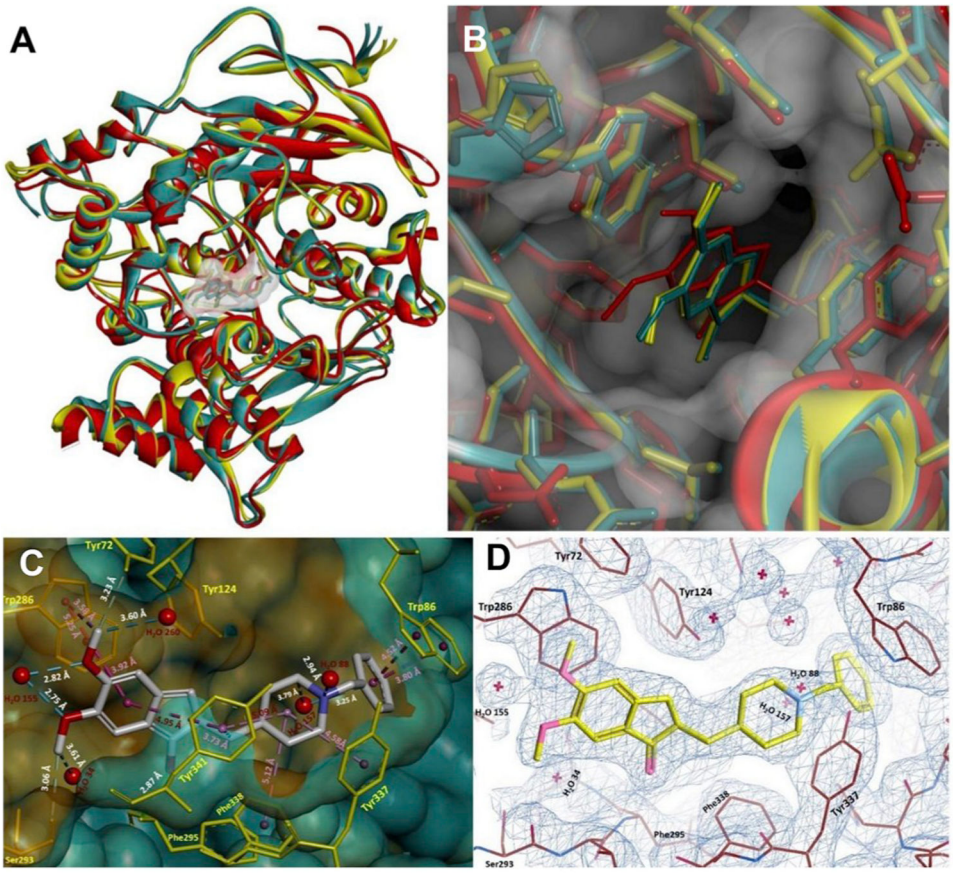

Fig. 4.

Donepezil*hAChE $P3_1$ complex (6O4W) monomer details (yellow ribbon) compared to $P3_121$ space group complexes 4EY7 (hAChE; teal ribbon) and 1EVE (TcAChE; red ribbon). **A)** Backbone Cα based overlay, **B)** Detail of donepezil bound in the AChE gorge opening. Connolly surfaces are from the $P3_1$ complex 6O4W. **C)** Distances of donepezil from stabilizing hAChE residues and **D)** $2F_o$-F_c electron density map (blue) contoured at 1σ level are given for the $P3_1$ complex. (For interpretation of the references to color in this figure legend, the reader is referred to the Web version of this article.)

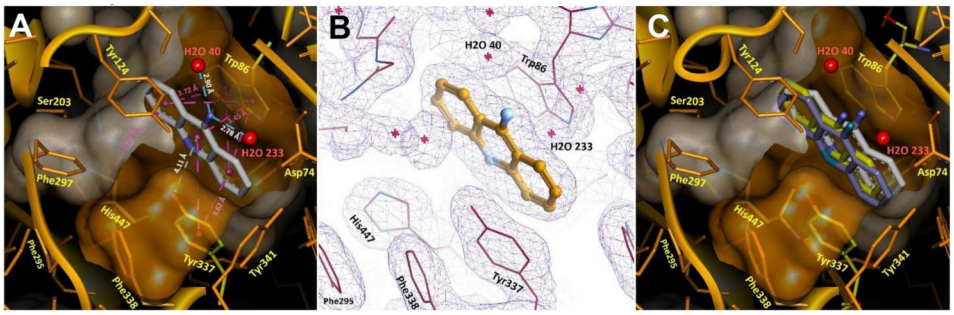

Fig. 5.

9-Aminoacridine*hAChE $P3_1$ complex (6O4X) **A)** stabilization details, and **B)** $2F_O$-F_C electron density map (blue) contoured at 1σ level. **C)** Binding positions of 9-aminoacridine (yellow sticks) and closely related tacrine molecules superimposed from the TcAChE complex (1ACJ; blue sticks) and hBChE complex (4BDS; white sticks) based on protein Cα overlays.

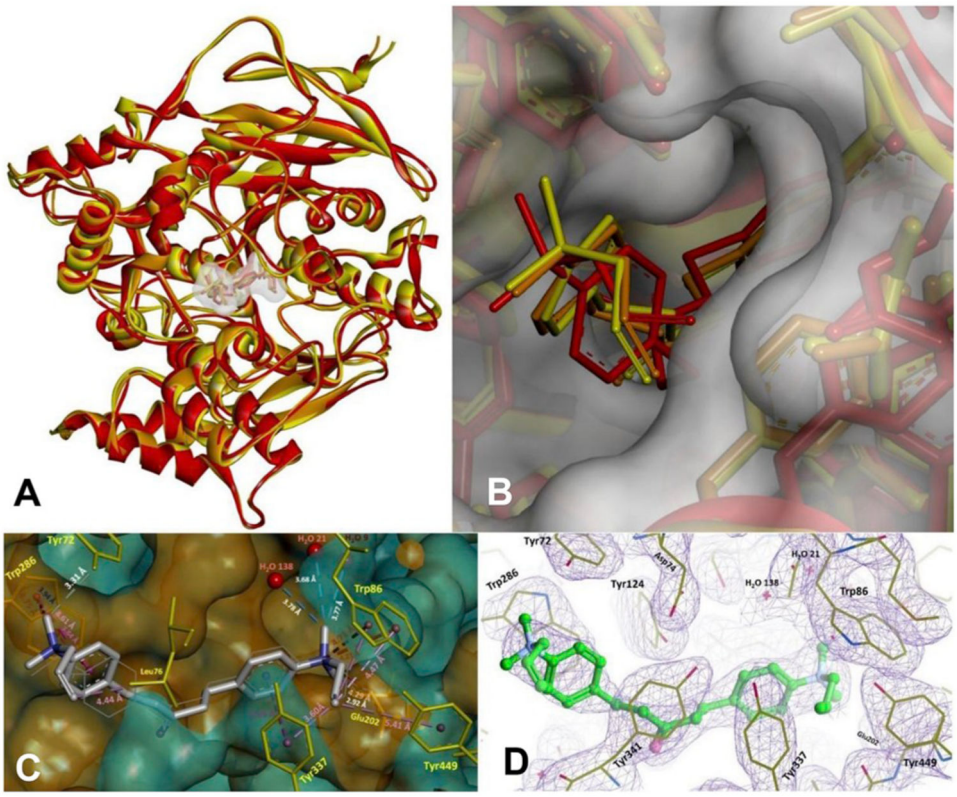

Fig. 6.

BW284c51*hAChE $P3_1$ complex 6O50 monomer details (yellow and orange ribbon for chains A and B compared to $P3_121$ space group TcAChE complex (1E3Q; red ribbon). **A)** Backbone Cα based overlay, **B)** Detail of BW284c51 bound in the AChE gorge opening. Connolly surfaces are from the $P3_1$ complex 6O50. **C)** Distances of BW284c51 from stabilizing hAChE residues in 6O50 and **D)** $2F_O$-F_C electron density map (blue) contoured at 1σ level of the $P3_1$ complex 6O50. (For interpretation of the references to color in this figure legend, the reader is referred to the Web version of this article.)

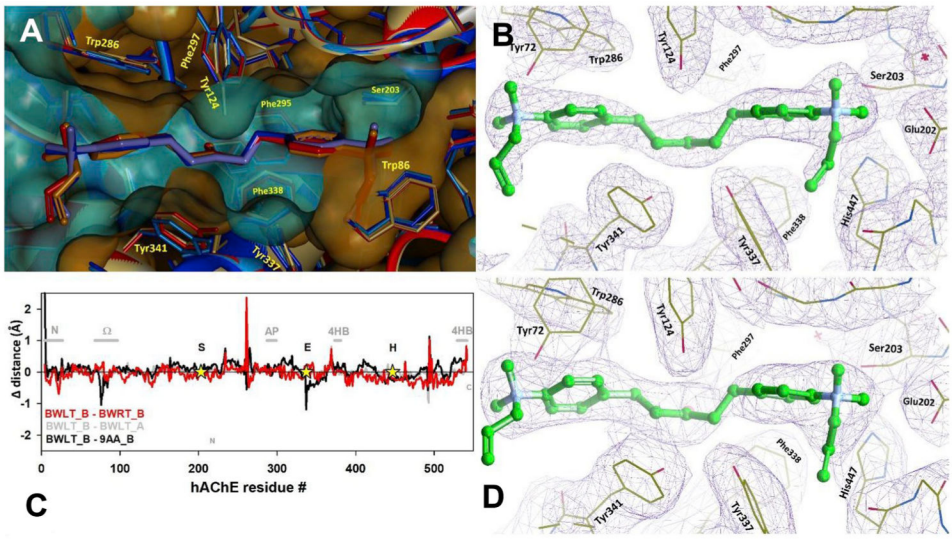

Fig. 7.

RT BW284c51*hAChE $P3_1$ complex structure (6O52) compared to the LT structure (6O50) of the same complex from Fig. 6. **A)** Cα-based overlay of four hAChE monomers, two from the RT structure (red and orange ribbon and sticks) and two from the LT structure (light and dark blue ribbon and sticks). **B)** The LT complex $2F_O$-F_C electron density map contoured at 1σ level and **D)** RT complex $2F_O$-F_C electron density map. **C)** The graph indicates the change in the distance of residue backbone Cα atoms from the Ser203 Cα compared to corresponding distances in the BW284c51*hAChE LT structure. Catalytic triad residues are indicated by stars and positions of the Ω loop, acyl pocket loop (AP), and 4HB α-helices (4HB) by horizontal grey bars. (For interpretation of the references to color in this figure legend, the reader is referred to the Web version of this article.)

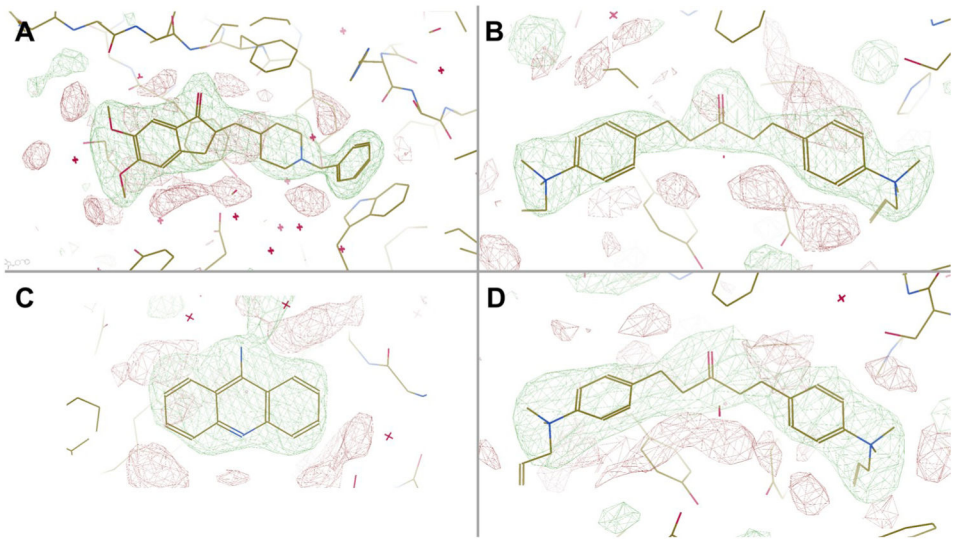

Fig. 8.

Simulated-annealing F_O-F_C omit maps of **A)** LT donepezil*hAChE complex (6O4W) contoured at 3 σ level. **B)** LT RT BW284c51*hAChE complex (6O50) contoured at 3 σ level **C)** LT 9-aminoacridine*hAChE complex (6O4X) density contoured at 3 σ level **D)** RT BW284c51*hAChE complex (6O52) contoured at 3 σ level.

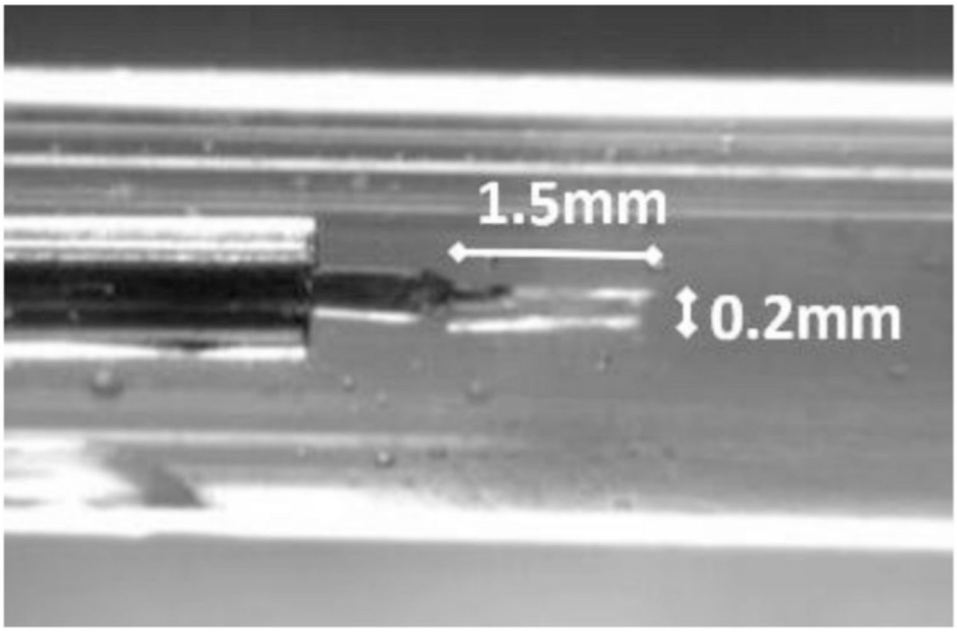

Image 1.

Photograph of large $P3_1$ crystal of hAChE*BW284c51 complex with dimensions 1.5 mm × 0.2 mm × 0.2 mm and estimated V = 0.06 mm^3. It was the only crystal in the crystallization drop. The crystal reached its full size in two months. Data were collected five months after the initiation of the crystallization experiment. Typical size of $P3_121$ hAChE crystals reported earlier [8] was 0.6 mm × 0.2 mm × 0.2 mm (V = 0.00024 mm^3), i.e. about 250-times smaller.

Table 1

X-ray crystallographic data collection and refinement statistics.

	LT			RT
	E2020	**9AA**	**BW**	**BW**
Data collection **Space group**		**$P3_1$**		**$P3_1$**
Cell dimensions:				
a, b, c (Å)	125.18, 125.18, 130.28	124.63, 124.63, 129.66	125.18, 125.18, 130.28	125.43, 125.43, 130.59
α, β, γ (°)		90, 90, 120		90, 90, 120
Wavelength	0.97919	0.97919	0.97919	0.97919
Resolution (Å)	40.00–2.35 (2.43–2.35)[a]	40.00–2.30 (2.38–2.30)	40.00–2.35 (2.43–2.35)	40.00–3.2 (3.31–3.2)
R_{merge}	0.030 (0.425)	0.041 (0.546)	0.026 (0.64)	0.099 (0.50)
R_{meas}	0.042 (0.598)	0.052 (0.711)	0.036 (0.907)	0.125 (0.658)
$R_{p.i.m.}$	0.030 (0.421)	0.032 (0.448)	0.026 (0.642)	0.075 (0.418)
$I/\sigma I$	12.5 (1.3)	14.4 (1.5)	14.5 (1)	7.1 (1.7)
Completeness (%)	92.1 (91.9)	78 (83.4)	80.1 (85.8)	81.1 (86.8)
Redundancy	1.8 (1.8)	1.6 (1.5)	1.2 (1.1)	2.3 (2.1)
Mosaicity	0.45	0.27	0.24	0.20
CC1/2	0.975 (0.642)	0.996 (0.448)	0.995 (0.395)	0.980 (0.636)
CC[a]	0.992 (0.884)	0.998 (0.787)	0.998 (0.752)	0.995 (0.882)
Refinement				
No. reflections	66738	73282	66738	29380
Resolution	27.92–2.35	31.46–2.30	27.92–2.35	39.17–3.2
*R*work/*R*free	0.204/0.245	0.190/0.223	0.204/0.245	0.153/0.189
No. atoms (non-H)	8681	8996	8681	8467
No. waters	379	556	217	31
R.m.s.d.				
Bonds (Å)	0.002	0.002	0.002	0.003
Bond angles (°)	0.606	0.533	0.606	0.551

Table 2

Analysis of dimerization interfaces identified in donepezil*AChE complexes from Fig. 1 by the PISA server. Estimated interface areas and solvation energies are indicated.

Dimer interface	6O4W (hAChE) $P3_1$	4EY7 (hAChE) $P3_121$	1EVE (TcAChE) $P3_121$
4-Helix Bundle (4HB)	1015 Å^2 −15 kcal/mol	988 Å^2 −14 kcal/mol	969 Å^2 −15 kcal/mol
Face to Face (FF)	617 Å^2 −4.5 kcal/mol	–	–
Face to Back (FB)	–	–	837 Å^2 −1.1 kcal/mol
Side to Side (SS)	–	332 Å^2 −3.4 kcal/mol	-

Table 3

Inhibition constants (nM) published for mouse AChE and BChE [14]. For donepezil, TcAChE and human BChE were used [3,15-17].

Enzyme	Donepezil		BW284c51		9-aminoaeridine		Tacrine	
	K_i	αK_i	K_i	αK_i	K_i	αK_i	K_i	αK_i
AChE	3.4	18	2.8	4.8	40	110	40	130
BChE	5760	nd	11 000	42 000	22	34	17	47

Table 4

RMSD values (in Å) for Cα-based overlay of 4HB dimers found in four $P3_1$ hAChE complexes (with 9AA, BW at LT, BW at RT and E2020; framed yellow) four $P3_121$ structures (4EY7 hAChE and TcAChE 1EVE, 1E3Q and 1ACJ; framed blue) and in tacrine*hBChE complex (4BDS).

	6O4X 9AA		**6O50 BW**		**6O52 BW_RT**		**6O4W E2020**		**4EY7 (E2020)**		**1EVE (E2020)**		**1E3Q (BW)**		**1ACJ (Tac)**		**4BDS (Tac)**		**Resolution (A)**
	$P3_1$	***hAChE***	***$P3_1$***	***hAChE***	***$P3_1$***	***hAChE***	***$P3_1$***	***hAChE***	***$P3_121$***	***hAChE***	***$P3_121$***	***TcAChE***	***$P3_121$***	***TcAChE***	***$P3_121$***	***TcAChE***	***I422***	***hBChE***	
6O4X 9AA	0.00		0.37		0.48		0.42		1.45		1.48		1.50		0.95		2.77		2.3
6O50 BW	0.37		0.00		0.38		0.49		1.49		1.53		1.52		0.97		2.68		2.4
6O52 BW_RT	0.48		0.38		0.00		0.63		1.49		1.49		1.46		0.90		2.69		3.2
6O4W E2020	0.42		0.49		0.63		0.00		1.52		1.56		1.62		1.06		2.69		2.4
4EY7 (E2020)	1.45		1.49		1.49		1.52		0.00		1.29		1.45		0.96		3.23		2.35
1EVE(E2020)	1.48		1.53		1.49		1.56		1.29		0.00		0.59		0.39		3.55		2.5
1E3Q (BW)	1.50		1.52		1.46		1.62		1.45		0.59		0.00		0.32		3.57		2.85
1ACJ (Tac)	0.95		0.97		0.90		1.06		0.96		0.39		0.32		0.00		2.75		2.8
4BDS (Tac)	2.77		2.68		2.69		2.69		3.23		3.55		3.57		2.75		0.00		2.1

Table 5

RMSD values (in Å) for Cα-based overlay of monomers found in four $P3_1$ hAChE complexes (with 9AA, BW at LT, BW at RT and E2020; framed yellow) four $P3_121$ structures (4EY7 hAChE and TcAChE 1EVE, 1E3Q and 1ACJ; framed blue) and in tacrine*hBChE complex (4BDS).

	6O4X_b 9AA		**6O4X_a 9AA**		**6O50_b BW**		**6O50_a BW**		**6O52_b BW_RT**		**6O52_a BW_RT**		**6O4W_b E2020**		**6O4W_a E2020**		**4EY7_b (E2020)**		**4EY7_a (E2020)**		**1EVE (E2020)**		**1E3Q (BW)**		**1ACJ (Tac)**		**4BDS (Tac)**		**Resolution (A)**
	P3$_1$	***hAChE***	***P3$_1$***	***hAChE***	***P3$_1$***	***hAChE***	***P3$_1$***	***hAChE***	***P3$_1$***	***hAChE***	***P3$_1$***	***hAChE***	***P3$_1$***	***hAChE***	***P3$_1$***	***hAChE***	***P3$_1$21***	***hAChE***	***P3$_1$21***	***hAChE***	***P3$_1$21***	***TcAChE***	***P3$_1$21***	***TcAChE***	***P3$_1$21***	***TcAChE***	***I422***	***hBChE***	
6O4X_b **9AA**	0.00		0.20		0.28		0.26		0.43		0.41		0.31		0.30		0.50		0.47		0.91		0.93		0.90		1.12		2.3
6O4X_a **9AA**	0.20		0.00		0.29		0.28		0.42		0.41		0.27		0.31		0.49		0.47		0.91		0.94		0.91		1.11		2.3
6O50_b **BW**	0.28		0.29		0.00		0.24		0.34		0.36		0.30		0.29		0.50		0.49		0.90		0.91		0.88		1.10		2.4
6O50_a **BW**	0.26		0.28		0.24		0.00		0.39		0.35		0.27		0.27		0.48		0.48		0.89		0.90		0.87		1.11		2.4
6O52_b **BW**_RT	0.43		0.42		0.34		0.39		0.00		0.29		0.41		0.42		0.51		0.53		0.86		0.86		0.84		1.05		3.2
6O52_a **BW**_RT	0.41		0.41		0.36		0.35		0.29		0.00		0.41		0.41		0.51		0.52		0.90		0.88		0.86		1.06		3.2
6O4W_b **E2020**	0.31		0.27		0.30		0.27		0.41		0.41		0.00		0.17		0.47		0.46		0.89		0.92		0.89		1.10		2.4
*6O4W*_a **E2020**	0.30		0.31		0.29		0.27		0.42		0.41		0.17		0.00		0.47		0.46		0.90		0.93		0.90		1.11		2.4
4EY7_b (E2020)	0.50		0.49		0.50		0.48		0.51		0.51		0.47		0.47		0.00		0.30		0.95		0.97		0.94		1.15		2.35
4EY7_a (E2020)	0.47		0.47		0.49		0.48		0.53		0.52		0.46		0.46		0.30		0.00		0.93		0.95		0.93		1.14		2.35
1EVE (E2020)	0.91		0.91		0.90		0.89		0.86		0.90		0.89		0.90		0.95		0.93		0.00		0.39		0.37		1.15		2.5
1E3Q (BW)	0.93		0.94		0.91		0.90		0.86		0.88		0.92		0.93		0.97		0.95		0.39		0.00		0.32		1.16		2.85
1ACJ (Tac)	0.90		0.91		0.88		0.87		0.84		0.86		0.89		0.90		0.94		0.93		0.37		0.32		0.00		1.15		2.8
4BDS (Tac)	1.12		1.11		1.10		1.11		1.05		1.06		1.10		1.11		1.15		1.14		1.15		1.16		1.15		0.00		2.1